Available online at www.sciencedirect.com

ScienceDirect

Procedia CIRP 00 (2022) 000–000

www.elsevier.com/locate/procedia

16th CIRP Conference on Intelligent Computation in Manufacturing Engineering, CIRP ICME '22, Italy

Spatial Annotation of Time Series for Data Driven Quality Assurance in Additive Manufacturing

Raven Reisch[a,b,*,+], Matteo Pantano[a,b,+], Lucas Janisch[a,c], Alois Knoll[b], Dongheui Lee[d]

[a] *Siemens AG, Otto-Hahn-Ring 6, 81739 Munich, Germany*
[b] *Technical University of Munich, Boltzmannstraße 4, Munich, Germany*
[c] *Friedrich-Alexander-Universität Erlangen-Nürnberg, Schloßplatz 4, Erlangen, Germany*
[d] *Technical University of Vienna, Karlsplatz 13, 1040 Wien, Austria*

* Corresponding author. Tel.: +49 (1522) 4725020; *E-mail raven.reisch@tum.de*
[+] The authors contributed equally

Abstract

One of the biggest challenges for artificial intelligence in industry is the lack of labeled application data. Particularly for time series data, labeling requires a large amount of time for data preparation and expert knowledge both in data analysis and in the application domain. In this work, we propose a methodology for labeling time series solving the two barriers identified above in an additive manufacturing use case. Our approach correlates spatial and temporal features of process defects by means of a spatial sensor. By applying our method, we were able to achieve shorter labeling time while obtaining high-quality labels.

Peer-review under responsibility of the scientific committee of the 16th CIRP Conference on Intelligent Computation in Manufacturing Engineering.

Keywords: Labeling, Time Series, Direct Energy Deposition, Quality Assurance, Spatio-Temporal, Spatial Sensors

1. Introduction

The lack of labeled application data is one of the major challenges for the adoption of machine learning based data analytics approaches in industry. Particularly for time series, creating labeled process data results in high costs as knowledge both in data analysis and in the application domain is needed. Additionally, a considerable amount of time should be invested, as certain aspects might not be visible in a single time series but only in a multivariate dataset.

Especially in Additive Manufacturing (AM), a high demand for labeled time series process data is apparent to develop and evaluate advanced monitoring setups which would enable the further industrialization of this process category. Relevant labels include defects as well as other deviations from the normal system behavior. To obtain information about the presence of these anomalies, a post-process quality assurance step is used. In general, the quality data is available as spatially resolved three-dimensional information for instance as point cloud of a scan using computer tomography (CT) or a laser scanner. However, a user-friendly method for mapping the spatially resolved quality data and the time series is needed.

This paper presents a straight-forward method for time series labeling based on spatial features in additive manufacturing use cases. By applying our method, we could achieve a shorter labeling time, a higher useability for the labeling expert as well as high-quality labels. The method is validated using a part that was built by means of a monitored Wire Arc Additive Manufacturing (WAAM) process.

The remainder of this paper is structured as follows. First, an overview of labeling technologies as well as basics in unsupervised and supervised data analytics are given. Subsequently, the methodology is presented. It is validated by testing the approach on the Wire Arc Additive Manufacturing

Peer-review under responsibility of the scientific committee of the 16th CIRP Conference on Intelligent Computation in Manufacturing Engineering.

use case. Finally, the results are discussed, and the paper is concluded by proposing directions for future work.

2. Related Work

To maintain the desired process behavior during the additive welding operation and thus produce the desired geometry, monitoring of the welding process is crucial. To achieve such goal, the main objective is to detect, control and predict process anomalies and geometry defects like delamination, oxidations, pores, geometrical deformations, or burn throughs that can occur due to improper process parameters or process instabilities. Regarding this, recent research was investigating various sensory systems, including camera observations of the wire tip [1] and the melt pool [2], [3] as well as spectrometers [4], and pyrometers [5]. Reisch et al. [6] developed a multivariate monitoring framework by using current and voltage surveillance combined with a wire feed speed sensor, gas flow sensor, welding camera, profile scanner, spectrometer, pyrometer, thermal imaging, and acoustic sensor.

To optimize and control the monitored process or to detect anomalies, the captured data needs to be made interpretable so that actual decisions or conclusions can be drawn from it. In other words, the data needs to be labeled. Especially with upcoming applications of machine learning methods in WAAM, the need for annotated data to train models like artificial neural networks (ANNs) becomes crucial.

An exemplary application of machine learning in WAAM is the work by Tang et al. [7] predicting the weld bead width and height with an ANN using temperature, wire feed rate, traveling speed as well as welding voltage and current for input data. To generate training data several single weld beads are created and subsequently scanned. The measured height and width were then manually correlated with the time series data measured during the process. A similar approach is presented also by Karmuhilan et al. [8].

ANNs are also applied when detecting faulty behavior in the melt pool images [2], [3], [9]. Publications covering this approach use several thousand images that are labeled with a class to then train a model. Also in related manufacturing methods like the keyhole TIG welding, the weld pool video stream is used to detect defects with machine learning methods [9].

To detect the defects on the manufactured geometry Li et al. [10] trained an object detection model to classify and locate defects relating to lack-of-fusion and voids immediately after the deposition of a layer. The future goal of the research team is to match the located defects with other quality monitoring signals. [10]

Alternatives to layer wise quality control of the finished parts are methods like optical inspection, crack detection, X-ray radiography, ultrasonic inspection and computed tomography. [11]

Despite the above-described approach by Li et al., the labelling of data in WAAM is done manually which is time-consuming and sometimes results in incomprehensive datasets and thus insufficiently trained models. As this is a general problem related research areas try to reduce the labelling effort by various approaches. To the best of the authors' knowledge, the publication most related to this work is presented by Gregorio et al. [12] in which a three-dimensional region of interest is labelled on the real object with an augmented reality pen. Once this is done a robot arm equipped with a camera can take a series of images of the object and automatically label them. However, this approach is not feasible for time series data which are the common type of data gathered by a monitoring system in WAAM.

3. Methodology

To overcome this issue, we propose a method which synchronizes spatial with temporal data. The synchronization is achieved through the following steps:

1. Temporal synchronization
2. TCP position adaption
3. Spatial defect annotation
4. Transformations
5. Proximity search
6. Postprocessing

In this section, a detailed description of the six steps is given.

3.1. Temporal synchronization

Time series which are obtained along the AM process, e.g., from sensors or numerical controls, are synchronized by using a system-wide global time reference. It is required to gather the tool center point (TCP) positions as time series data.

3.2. TCP position adaption

In the AM process, deviations can occur between the nominal and the actual TCP positions. Real-time measurements of these deviations are used to adjust the TCP time series accordingly. In WAAM, these measurements can be done for instance by a machine learning based nozzle-to-work distance measurement [13]. In laser assisted AM processes such as Laser Metal Deposition (LMD) an optical coherence tomography could be used [14].

3.3. Spatial defect annotation

In the post-process quality assurance, defects in the final part are detected and are assigned to coordinates in a reference coordinate system. This can be done by using the voxel number in a CT scan or the physical coordinates of defects which are annotated with a virtual reality (VR) tracker as described in Sec. 3.4. The tracker used in this work is the Tracepen™ from the company Wandelbots™. The tracking system is based on the principle of reflecting photodiode sensors which receive an infrared signal and send it back to a tracking station to measure distance of the tracker to a reference system. Due to this working principle the position of the tracker is expressed in relation to the tracking station [15].

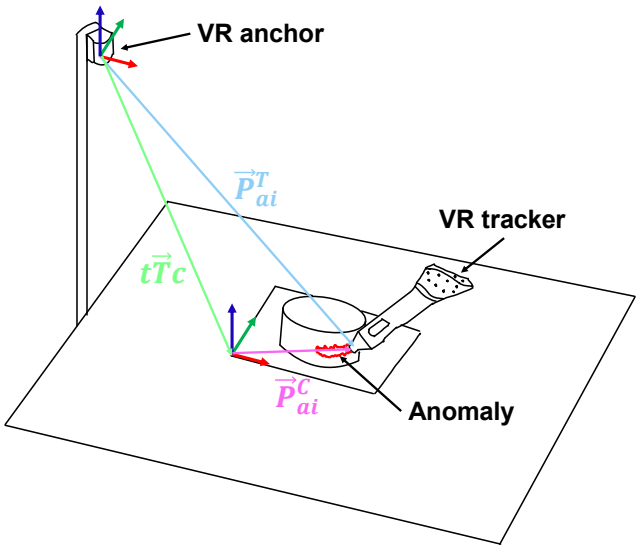

Figure 1: Transformations for obtaining the anomalies coordinates in the component coordinate system. The VR tracker points to the anomaly and defines its position on the coordinate system of the VR anchor $\vec{P}^T_{ai}$. Such coordinates are transformed to the component coordinate system through the transformation $t\vec{T}c$. Finally, the anomaly is defined in the component coordinate system $\vec{P}^C_{ai}$.

3.4. Transformations

The obtained defect coordinates are transferred from the reference coordinate system to the component coordinate system using a coordinate transformation.

In case of the CT scan-based defect coordinates, this coordinate transformation is done by simply applying a rotation and a translation to the defect positions. In case of the VR tracker, additional steps must be conducted to gather defect coordinates in the part coordinate system. The problem is shown in Figure 1. Therefore, using the nomenclature of the figure, the transformation $t\vec{T}c$ had to be calculated. For this calculation an approach like the one proposed by Zhang et al. [16] was followed. Therefore, the VR tracker was used to sample three points from the component through its coordinate system. More precisely, the origin ($\vec{P}^T_{u1}$), a point along the x-axis ($\vec{P}^T_{u2}$), and a point in the x-y plane ($\vec{P}^T_{u3}$) of the component coordinate system. Afterwards, by assuming the following for the selected points in the component coordinate system:

$$\vec{P}^C_{u1} = [0; 0; 0] \quad (1)$$

$$\vec{P}^C_{u2} = [x_{u2}; 0; 0] \quad (2)$$

$$\vec{P}^C_{u3} = [x_{u3}; y_{u3}; 0] \quad (3)$$

The following equation can be solved for $t\vec{T}c$:

$$\vec{P}^T_{ui} = t\vec{T}c\ \vec{P}^C_{ui}, \forall i \quad (4)$$

Finally, knowing the transformation $t\vec{T}$ and calculating its inverse $c\vec{T}t$, the points of any anomaly can be defined by:

$$\vec{P}^C_{ai} = c\vec{T}t\ \vec{P}^T_{ai}, \forall i \quad (5)$$

3.5. Proximity search

The mapping between the spatially annotated defects and the times series takes place by annotating the TCP time series based on the spatial proximity of the transformed defect coordinates.

Therefore, the Euclidian distance between every labeled defect position x_{di}, y_{di}, z_{di} and the TCP positions x_i, y_i, z_i within the TCP time series is calculated.

$$d = \sqrt{(x_i - x_{di})^2 + (y_i - y_{di})^2 + (z_i - z_{di})^2} \quad (6)$$

If the distance is smaller than a tolerance value d_{tol}, the data point is labeled as anomalous. d_{tol} is influenced by various factors such as the spatial annotation accuracy of the labeling expert or the spatial accuracy of the spatial sensor. However, a lower boundary can be defined which ensures that every labeled defect can be related to a monitored TCP position. The boundary value depends on the sample rate f_{pos} of the TCP time series, the maximum TCP velocity v_{TCP} in the process, the hatching distance d_h and the maximum layer height d_l:

$$d_{tol} \geq \sqrt{\left(\frac{v_{TCP}}{2 \cdot f_{pos}}\right)^2 + \left(\frac{d_l}{2}\right)^2 + \left(\frac{d_h}{2}\right)^2} \quad (7)$$

To reduce the computational time complexity of the proximity search, a binary search using cubical regions can be used [17].

3.6. Postprocessing

At last, the annotations of the TCP time series are transferred to other synchronized time series. In case of different sample rates, the annotations are interpolated along the time.

4. Results and Discussion

4.1. Test methodology

To evaluate the methodology, a sample part with helical path and forced anomalies was built using the WAAM process. The anomalies were forced by reducing the gas flow in the process, resulting in heavy oxidation and slag. Additionally, a discontinuity was introduced in the first revolution of the helix which propagated in the next four layers. Along the process,

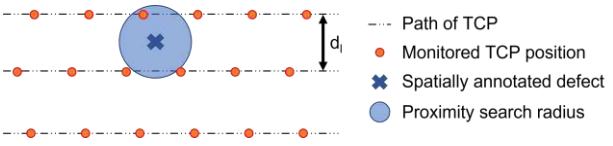

Figure 2: Proximity search for spatial correlation between TCP positions in the time series and the spatially annotated defects. The minimum radius for the search depends on the spatial resolution of the TCP position measurements and the layer height.

Figure 4: Spatially annotating the defects in the sample part using the VR tracker by Wandelbots™. The obtained coordinates must be transferred from the tracker coordinate system to the component coordinate system using coordinate transformations.

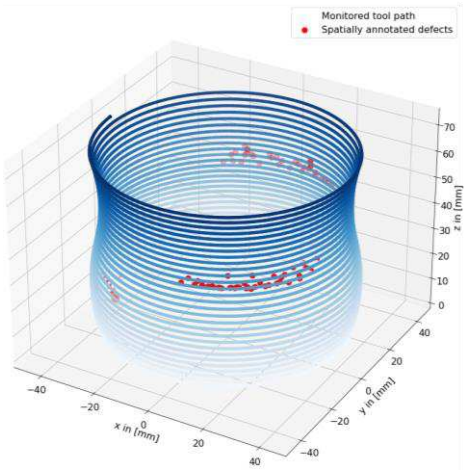

Figure 3: Spatially annotated defects visualized in red after the coordinate transformation in the component coordinate system along the monitored, adapted tool path (blue).

the TCP positions as well as the voltage data were monitored. The defects in the final part were labeled using a CT scan and a VR tracker as shown in Figure 4.

The spatial annotations of the time series were validated using an unsupervised anomaly detection approach based on a sliding moving average (see [17]).

4.2. Labelling accuracy

In Figure 3, the tool path based on the monitored TCP positions is visualized in blue. As the tool path was following a helical path, the height of the spiral was scaled depending on the final parts height to adapt the TCP positions according to step 2. In red, the spatially annotated defects are visualized. Beforehand, their coordinates were transformed from the reference coordinate system in the CT scan to the component coordinate system.

Having the transformed defect labels and the adapted TCP time series, the proximity search was conducted using a sphere radius of 1.4 mm. Finally, the annotations were transferred to the synchronized voltage times series. As shown in Figure 5 qualitatively, the yellow spatially annotated defects correspond to the outliers in the voltage time series. Also, the consequential defects were detected and labeled. The discontinuity in the first revolution which propagated in the next four layers was annotated spatially but couldn't be detected with the anomaly detection approach.

A quantitative analysis of the automated and the spatial annotation method for labelling the datapoints in the print job is shown in the confusion matrix in Table 1.

Table 1: Confusion matrix of annotated datapoints comparing the automated and the spatial annotation method. Many datapoints were labelled as abnormal by the spatial annotation which were not detected by the anomaly detection.

		Automated annotation	
		Normal	Abnormal
Spatial annotation	Normal	5792784	69723
	Abnormal	189000	50836

The normal process behavior was labeled as normal by both methods simultaneously most of the times, resulting in a high accuracy score of 0.96.

However, in case of abnormal annotations, the methods differ significantly from one another, resulting in a balanced accuracy score of only 0.69. On the one hand, datapoints were spatially annotated as abnormal but were not highlighted in the automated annotation. There were several defects such as the discontinuity in the first five layers or the slag in the revolutions after the heavy oxidations which were not reliably detected. Additionally, the proximity search results in a spatial blurriness

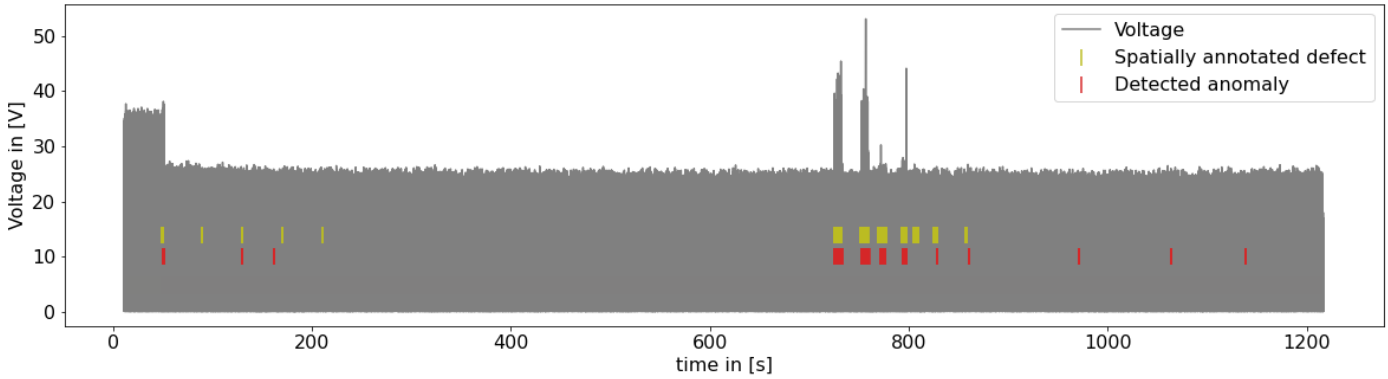

Figure 5: Labelled voltage time series. The green labels were annotated by means of the spatial annotation approach while the red ones were created using an unsupervised anomaly detection method.

in the annotation. Thus, more datapoints might be annotated than needed. On the other hand, the anomaly detection detected an abnormal behavior which was not annotated spatially. Some unusual process behavior doesn't result in defects. Thus, the data looks abnormal, but a defect is not present. Using a combined spatial and automated annotation could ensure, that less unknown abnormal datapoints can be found in a training set for semi-supervised learning. Hereby, both the process perspective in terms of data anomalies as well as the quality perspective in terms of defects is considered. Additionally, while the automated annotation is only capable of annotating anomalous behavior, the spatial annotation enables the labeling of specific defect types in AM.

To investigate further the capability of the labelling approach a preliminary user test with two operators was conducted. The results of the user test are shown in Table 2. The user test includes a comparison between a defect labeling based on the spatial annotation and one based on a tool for time series labeling. The spatial labeling was conducted using the VR tracker with the real part or a CT-scan. The temporal labeling was based on the voltage and current time series. The users had 10 minutes to label the defects, both for the spatial and for the temporal annotation methods. The labeling methods were evaluated regarding their usability and labeling performance. The ground-truth for the calculation of the recall, precision, F1 score and balanced accuracy metrics was created by a combination of manual labeling conducted by a process expert both in space and time and of an automated labeling using a supervised anomaly detector.

Table 2: Comparison of annotation methods using the spatial annotation (with the VR tracker and CT scan) and the temporal annotation (time series of voltage, current, structural acoustic). The users had to a label a cone which was previously labelled by an expert and a supervised anomaly detector in 10 min.

Annotation method	Spatial annotation				Temporal annotation	
	CT-Scan		VR tracker			
User	1	2	1	2	1	2
Usability of method	8	8	9	9	1	5
Confidence in finding all defects	9	8	8	7	2	3
Confidence in label precision	6	6	6	5	4	6
Recall	.41	.43	.11	.50	.25	.34
Precision	.44	.43	.08	.15	.84	.48
F1 Score	.43	.42	.09	.24	.39	.40
Balanced accuracy	.67	.70	.52	.68	.62	.66

In all cases, the usability and the confidence in finding all defects was higher for the spatial annotation. It is necessary to mention, that even if the user had 10 minutes to conduct the labeling, the users were finished using the spatial annotation in average already after 5 minutes. The confidence in the precision of the labels was similar for all annotation methods.

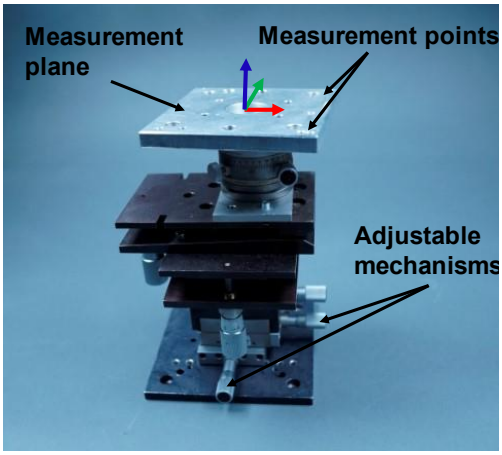

Figure 6: Test bench for the evaluation of the accuracy of the VR tracker. The test bench was composed of a measurement plane mounted on mechanical mechanisms to induce controlled translations of the measurement plane. To measure the accuracy the VR tracker was used to sample some points of the measurement plane and measured translations were compared with indicators in the adjustable mechanisms.

Regarding the labeling performance, the spatial annotations showed a high recall. However, the precision was very low, which can be ascribed to the spatial blurriness due to the proximity radius. The F1-score and the balanced accuracy is higher for the spatial annotation methods. These results of the preliminary study support the previously mentioned recommendation to combine spatial and temporal labeling. First, a preselection of relevant areas in the part and in the time could be done by the spatial annotation of the time series. Then, the labeling is optimized by focusing on the highlighted areas in the time series. This approach could reduce the labeling time and improve the recall and the precision of the labeling. However, further user tests should be carried out to better generalize the findings of this approach due to variabilities in the performances depending on the user as shown from the two tests conducted with the VR tracker.

4.3. Spatial resolution of VR tracker

To evaluate the precision of the transformation and of the VR tracker a comparison test with a test bench was performed. More precisely, a test bench composed of a plane with mechanical mechanisms to induce controlled and precise translations on the three axis was used. A picture of the test bench used is shown in Figure 6. With the test bench-controlled transformations were performed and measured through the labels of the mechanical mechanisms. After each transformation, three points (origin, x-axis and xy-plane) were sampled to calculate transformations given from the VR tracker and compared with the labels of the control mechanism. This evaluation yielded that the translation on the x-axis, y-axis and z-axis have no discrepancy with the ground truth from the control mechanisms. However, the precision was measured on the millimetric scale due to limitations on the evaluations' tool. Therefore, some accuracy errors could be present in the sub-millimeter scale. Moreover, it is worth mentioning that the tip

used for the defect labelling during the user testing had a circular diameter of 5mm. Therefore, considering the approach described in Sec. 3.5 with a labelling radius of 1.4mm it is easy to note that the user could make labelling errors due to the required high precision. This somehow explains the low precision and achieved in the user testing above. Therefore, the authors suggest that the approach with the VR tracker as spatial sensor should be used accordingly to the part and anomaly size or within a hybrid approach with temporal labelling as mentioned before.

Table 3: Summary of the finding related to the evaluation of the accuracy of the VR tracker. The VR tracker showed a good accuracy in the millimetric scale showing no discrepancy compared to the test bench. However, errors under the millimetric scale could not be measured due to limitations of the evaluations' tool.

Transformation	Ground truth	Measured
X translation	5 mm	5 mm
Y translation	5 mm	5 mm
Z translation	3 mm	3 mm

5. Conclusion

In this paper, we proposed a method for spatially annotating time series. Our approach correlates spatial and temporal features of process defects by means of a proximity search and geometrical transformations. By applying our method on a use case with a preliminary user test, we could achieve higher usability and shorter labeling time while obtaining high-quality labels. The testing was limited by the number of involved users and the minimum detectable defect through the spatial approach due to employed hardware. Therefore, to demonstrate the generalizability of our findings future research could elaborate on the use of the spatial annotation with semiautomated labeling to accelerate the data analytics in different AM monitoring use cases. For example, the proposed method can be transferred to any other multi-axis-based AM technologies, including other Direct Energy Deposition technologies such as Laser Metal Deposition, as well as material extrusion and fused deposition modeling.

Acknowledgements

The authors gratefully acknowledge funding from EIT RawMaterials for the project SAMOA - Sustainable Aluminium additive Manufacturing fOr high performance Applications, no. 18079.

References

[1] Q. Zhan, Y. Liang, J. Ding, und S. Williams, „A wire deflection detection method based on image processing in wire + arc additive manufacturing“, *Int J Adv Manuf Technol*, Bd. 89, Nr. 1–4, S. 755–763, März 2017, doi: 10.1007/s00170-016-9106-2.

[2] H.-W. Cho, S.-J. Shin, G.-J. Seo, D. B. Kim, und D.-H. Lee, „Real-time anomaly detection using convolutional neural network in wire arc additive manufacturing: Molybdenum material“, *Journal of Materials Processing Technology*, Bd. 302, S. 117495, Apr. 2022, doi: 10.1016/j.jmatprotec.2022.117495.

[3] C. Lee, G. Seo, D. B. Kim, M. Kim, und J.-H. Shin, „Development of Defect Detection AI Model for Wire + Arc Additive Manufacturing Using High Dynamic Range Images“, *Applied Sciences*, Bd. 11, Nr. 16, S. 7541, Aug. 2021, doi: 10.3390/app11167541.

[4] Z. Zhao, Y. Guo, L. Bai, K. Wang, und J. Han, „Quality monitoring in wire-arc additive manufacturing based on cooperative awareness of spectrum and vision“, *Optik*, Bd. 181, S. 351–360, März 2019, doi: 10.1016/j.ijleo.2018.12.071.

[5] C. Halisch, T. Radel, D. Tyralla, und T. Seefeld, „Measuring the melt pool size in a wire arc additive manufacturing process using a high dynamic range two-colored pyrometric camera“, *Weld World*, Bd. 64, Nr. 8, S. 1349–1356, Aug. 2020, doi: 10.1007/s40194-020-00892-5.

[6] R. Reisch, T. Hauser, B. Lutz, M. Pantano, T. Kamps, und A. Knoll, „Distance-Based Multivariate Anomaly Detection in Wire Arc Additive Manufacturing“, in *2020 19th IEEE International Conference on Machine Learning and Applications (ICMLA)*, Miami, FL, USA, Dez. 2020, S. 659–664. doi: 10.1109/ICMLA51294.2020.00109.

[7] S. Tang, G. Wang, H. Song, R. Li, und H. Zhang, „A novel method of bead modeling and control for wire and arc additive manufacturing“, *RPJ*, Bd. 27, Nr. 2, S. 311–320, März 2021, doi: 10.1108/RPJ-05-2020-0097.

[8] M. Karmuhilan und A. kumar sood, „Intelligent process model for bead geometry prediction in WAAM“, *Materials Today: Proceedings*, Bd. 5, Nr. 11, S. 24005–24013, 2018, doi: 10.1016/j.matpr.2018.10.193.

[9] C. Xia, Z. Pan, Z. Fei, S. Zhang, und H. Li, „Vision based defects detection for Keyhole TIG welding using deep learning with visual explanation“, *Journal of Manufacturing Processes*, Bd. 56, S. 845–855, Aug. 2020, doi: 10.1016/j.jmapro.2020.05.033.

[10] Y. Li *u. a.*, „Towards Intelligent Monitoring System in Wire Arc Additive Manufacturing: A Surface Anomaly Detector on a Small Dataset“, In Review, preprint, Dez. 2021. doi: 10.21203/rs.3.rs-1165098/v1.

[11] K. Treutler und V. Wesling, „The Current State of Research of Wire Arc Additive Manufacturing (WAAM): A Review“, *Applied Sciences*, Bd. 11, Nr. 18, S. 8619, Sep. 2021, doi: 10.3390/app11188619.

[12] D. De Gregorio, A. Tonioni, G. Palli, und L. Di Stefano, „Semi-Automatic Labeling for Deep Learning in Robotics“, *arXiv:1908.01862 [cs]*, Aug. 2019, Zugegriffen: 4. März 2022. [Online]. Verfügbar unter: http://arxiv.org/abs/1908.01862

[13] R. T. Reisch *u. a.*, „Nozzle-to-Work Distance Measurement and Control in Wire Arc Additive Manufacturing“, in *2021 2nd European Symposium on Software Engineering*, Larissa Greece, Nov. 2021, S. 163–172. doi: 10.1145/3501774.3501798.

[14] M. Kogel-Hollacher, M. Strebel, C. Staudenmaier, und D. Regulin, „OCT sensor for layer height control in DED using SIEMENS machine controller“, S. 4, 2020.

[15] A. K. T. Ng, L. K. Y. Chan, und H. Y. K. Lau, „A low-cost lighthouse-based virtual reality head tracking system“, in *2017 International Conference on 3D Immersion (IC3D)*, Brussels, Dez. 2017, S. 1–5. doi: 10.1109/IC3D.2017.8251910.

[16] W. Zhang, X. Ma, L. Cui, und Q. Chen, „3 Points Calibration Method of Part Coordinates for Arc Welding Robot“, in *Intelligent Robotics and Applications*, Bd. 5314, C. Xiong, Y. Huang, Y. Xiong, und H. Liu, Hrsg. Berlin, Heidelberg: Springer Berlin Heidelberg, 2008, S. 216–224. doi: 10.1007/978-3-540-88513-9_24.

[17] R. T. Reisch *u. a.*, „Context awareness in process monitoring of additive manufacturing using a digital twin“, *Int J Adv Manuf Technol*, Jan. 2022, doi: 10.1007/s00170-021-08636-5.